




Refined Ischemic Penumbra Imaging with Tissue pH and Diffusion Kurtosis Magnetic Resonance Imaging

Jesse Cheung^{1,2} · Madeline Doerr^{2,3} · Ranliang Hu⁴ · Phillip Zhe Sun^{2,4} 

Received: 12 February 2020 / Revised: 14 October 2020 / Accepted: 18 October 2020 / Published online: 7 November 2020
© Springer Science+Business Media, LLC, part of Springer Nature 2020

Abstract

Imaging has played a vital role in our mechanistic understanding of acute ischemia and the management of acute stroke patients. The most recent DAWN and DEFUSE-3 trials showed that endovascular therapy could be extended to a selected group of late-presenting stroke patients with the aid of imaging. Although perfusion and diffusion MRI have been commonly used in stroke imaging, the approximation of their mismatch as the penumbra is oversimplified, particularly in the era of endovascular therapy. Briefly, the hypoperfusion lesion includes the benign oligemia that does not proceed to infarction. Also, with prompt and effective reperfusion therapy, a portion of the diffusion lesion is potentially reversible. Therefore, advanced imaging that provides improved ischemic tissue characterization may enable new experimental stroke therapeutics and eventually further individualize stroke treatment upon translation to the clinical setting. Specifically, pH imaging captures tissue of altered metabolic state that demarcates the hypoperfused lesion into ischemic penumbra and benign oligemia, which remains promising to define the ischemic penumbra's outer boundary. On the other hand, diffusion kurtosis imaging (DKI) differentiates the most severely damaged and irreversibly injured diffusion lesion from the portion of diffusion lesion that is potentially reversible, refining the inner boundary of the penumbra. Altogether, the development of advanced imaging has the potential to not only transform the experimental stroke research but also aid clinical translation and patient management.

Keywords Acute stroke · Acidification · Diffusion kurtosis imaging (DKI) · MRI mismatch · Penumbra · pH MRI

Introduction

Stroke is one of the primary causes of adult mortality, morbidity, and disability [1, 2]. Ischemic stroke is caused by a vascular blockage that results in sudden and severe hypoperfusion, leading to neurologic dysfunctions and brain tissue injury. The most severely hypoperfused brain tissue forms a core of irreversible damage (infarction), and the surrounding

hypoperfused area is at risk of infarction (penumbra). If cerebral perfusion is not restored promptly, the infarction core may expand over time to the hypoperfused territory [3]. The goal of acute stroke treatment is to rapidly and safely recanalize the occluded vessel(s), salvage ischemic tissue, prevent infarct growth, and minimize hemorrhagic complications [4–6].

The Transition from Stroke Onset Time Clock– to Tissue Clock–Based Treatment

Intravenous tissue plasminogen activator (IV tPA) administered within the first 4.5 h of stroke onset has been and continues to be the standard care of acute stroke treatment [7]. tPA restores perfusion and improves functional outcomes by inducing fibrin degradation to break down the blood clot. However, tPA's therapeutic time window is very narrow, limiting it to a very small group of stroke patients. Although time is critical, there has been tremendous interest in individualizing stroke therapy by transitioning from stroke onset time–based treatment (time clock) to salvageable tissue–based

Jesse Cheung and Madeline Doerr contributed equally to this work.

✉ Phillip Zhe Sun
pzhesun@emory.edu

¹ Emory College of Arts and Sciences, Emory University, Atlanta, GA 30329, USA

² Yerkes Imaging Center, Yerkes National Primate Research Center, Emory University, Atlanta, GA 30329, USA

³ Dartmouth College, Hanover, NH 03755, USA

⁴ Department of Radiology and Imaging Sciences, Emory University School of Medicine, 1364 Clifton RD NE, Atlanta, GA 30322, USA

patient enrollment (tissue clock) [8, 9]. The key is to identify stroke patients with substantial penumbra tissue who are likely to benefit from reperfusion treatment [10]. Recent DAWN [11] and DEFUSE-3 [12] trials have shown that imaging-guided late-window recanalization is beneficial in carefully selected large vessel occlusion (LVO) stroke patients. Although routine stroke imaging has been well established in stroke clinical trials, it has been recognized that there are limitations. Patients in the DAWN trial had relatively small infarctions (average core < 10 ml). The majority of stroke patients (~ 70%) presenting 6–24 h with NIH stroke scale (NIHSS) over 6 are not DAWN and DEFUSE-3 eligible [13]. As Fisher and Xiong pointed out, it is urgent to determine both the lowest Alberta stroke program early CT score (ASPECTS) and the largest ischemic core volume where thrombectomy is no longer beneficial [14]. The ASPECTS is calculated by deducting 1 point from a score of 10 points for any evidence of early ischemic change for each of the defined regions, which provides a quantitative topographic CT score of acute stroke.

MRI has also been recently shown in the WAKE-UP trial to be useful in guiding tPA thrombolysis in stroke patients with unknown stroke onset time [15]. In this study, the presence of diffusion-weighted imaging (DWI) lesion and the absence of parenchymal hyperintensity on fluid-attenuated inversion recovery (FLAIR) MRI were used as a surrogate marker for early infarction amenable to thrombolytic therapy. However, many patients with early infarcts may be excluded by this approach since FLAIR hyperintense lesion can occur in 15% of patients imaged under 3 h and in 41% of patients imaged at 3 to 4.5 h [16]. A more accurate tissue marker has tremendous potential to improve selection in patients with unknown stroke onset time. Furthermore, a more tissue-specific imaging marker may also be helpful in evaluating strokes that do not arise from anterior circulation large vessel occlusions. For example, lacunar-type and posterior fossa infarctions may have different imaging characteristics than anterior circulation territorial infarctions [17].

Stroke Imaging

Imaging has played a crucial role in identifying acute stroke patients for thrombolytic and endovascular treatments [18]. There are four essential tasks of acute stroke imaging: to detect the presence of hemorrhage, to identify the location and severity of occlusion(s), to measure infarct core volume, and to estimate the penumbral tissue [10, 19]. Both CT and MRI have advantages and disadvantages in stroke imaging [20–24]. CT is currently the most commonly used imaging modality due to its wide availability and rapid acquisition. On the other hand, MRI is versatile and can characterize the hemodynamic, metabolic, and structural status of the ischemic tissue, which provides a comprehensive characterization of

the ischemic core and penumbra [25, 26]. Whereas MRI exams may take longer than CT, it is worth noting that fast stroke MRI protocols with good diagnostic quality have been performed in scan times rivaling that of CT protocols for the evaluation of acute stroke patients [27].

Acute ischemia induces a cascade of tissue changes (Fig. 1), depending on the level and duration of hypoperfusion [28–30]. Ischemic tissue initially suffers from disrupted gene expression and protein synthesis under the condition of mild hypoperfusion (35–50 ml/100 g/min). Such changes are, however, not detectable using non-invasive imaging. With the further reduction in perfusion, ischemic tissue transitions from aerobic to anaerobic glycolysis and causes changes in cerebral metabolic rate of glucose (CMRG) and lactate production (25–35 ml/100 g/min). Although MR spectroscopy, such as ^1H and phosphorous ^{31}P MRS, can detect such metabolite changes, the spatiotemporal resolution of MRS is not sufficient for acute stroke imaging [31–34]. Upon metabolic disruption, ischemic tissue becomes acidic (lactic acidosis) with glutamate release, which represents a narrow range of perfusion thresholds between selective neuronal loss (25–50 ml/100 g/min) and infarction (under 22 ml/100 g/min) [35–39]. With a further reduction of perfusion level, key tissue metabolites such as phosphocreatine and adenosine triphosphate (ATP) deplete, which quickly leads to irreversible tissue injury and infarction. It is critical for stroke imaging to capture events along this cascade of worsening tissue damage so that

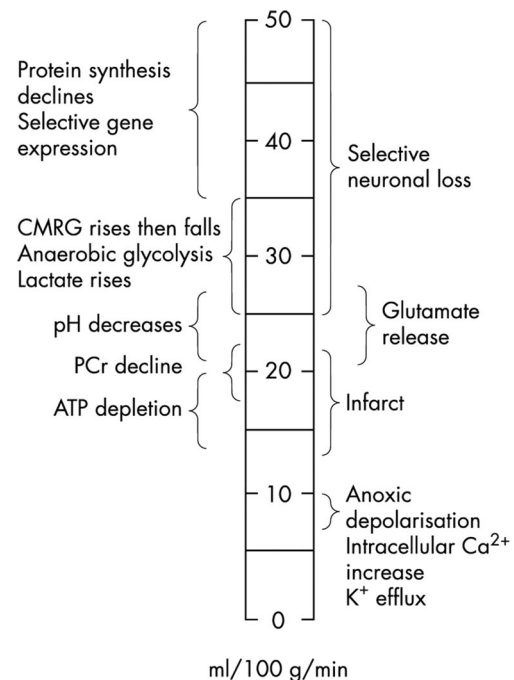


Fig. 1 A diagram of ischemic tissue injury cascades following acute stroke. Note that the glucose metabolism, lactate, and pH changes occur before infarction, suggesting that such indices are biomarkers for defining ischemic penumbra (Markus HS. *J Neurol Neurosurg Psychiatry*. 2004;75(3):353–61)

the ischemic tissue can be staged correctly in real time for individualizing stroke therapy.

Diffusion and Perfusion MRI

DWI is currently the operational gold standard for defining the ischemic core [8, 40]. It has been documented that the ischemic core has a reduced apparent diffusion coefficient (ADC) for the first 7 days, followed by ADC normalization and subsequent increases above that of healthy tissue [41]. Within the first hours of stroke onset, DWI is the most sensitive and specific means of depicting the extent and size of infarction. It has been relied upon to establish the infarction volume thresholds in which recanalization will likely be futile and risky if above [42, 43]. Perfusion-weighted MRI (PWI) can be performed using either contrast-enhanced or non-contrast methods to depict the severity of ischemia [44–48]. Whereas arterial spin labeling (ASL) perfusion MRI provides superior perfusion measurement, it is often technically challenging in the acute stroke setting, and dynamic susceptibility contrast (DSC) MRI is more widely used [49–51]. In the absence of revascularization, the infarction may grow from the initial DWI lesion to approach the PWI lesion. It is worth noting that not all hypoperfusion lesions will proceed to infarction, likely because the collateral circulation can sustain the ischemic tissue and, therefore, slow down or even prevent infarction growth [52]. Altogether, DWI and PWI lesion mismatch has been postulated as an operational penumbra to identify stroke patients for reperfusion treatment in an extended time window [53].

Limitation of Routine Diffusion and Perfusion MRI

Although diffusion and perfusion imaging has been widely used, the perfusion/diffusion (PWI/DWI) lesion mismatch paradigm is oversimplified. The mismatch could not adequately depict the heterogeneity of the viable ischemic tissues [54]. The PWI/DWI mismatch may not only contain a mixture of penumbral and benign oligemic tissue but also fail to include a portion of the reversible diffusion lesion. Specifically, the perfusion thresholds for ischemic injury varies with sex, age, and tissue type (gray versus white matter) [55–58]. The perfusion lesion often overestimates the penumbra by including the mild ischemic area unlikely to infarct (benign oligemia) [59]. On the other hand, the DWI lesion suffers from graded metabolic disruption and could overestimate the ischemic core [60–62]. A portion of the DWI lesion is reversible with early thrombolysis, even in cases with large DWI lesions [63–66]. Whereas DWI reversal had been considered infrequent [67], recent studies revived the concept of DWI renormalization in patients with early recanalization [68]. For example, Hsia et al. pointed out, “Apparent diffusion coefficient (ADC) evolution in patients with early, complete

revascularization, now more commonly seen with endovascular therapy, is strikingly different from our historical understanding.” [69]. The study concluded that recanalization and reperfusion lead to an earlier increase in intensity and a more rapid ADC normalization of the ischemic core than before. Early revascularization and ADC normalization often occur together, which may serve as a potential biomarker for developing future adjunctive treatment.

The Refined Mismatch Paradigm

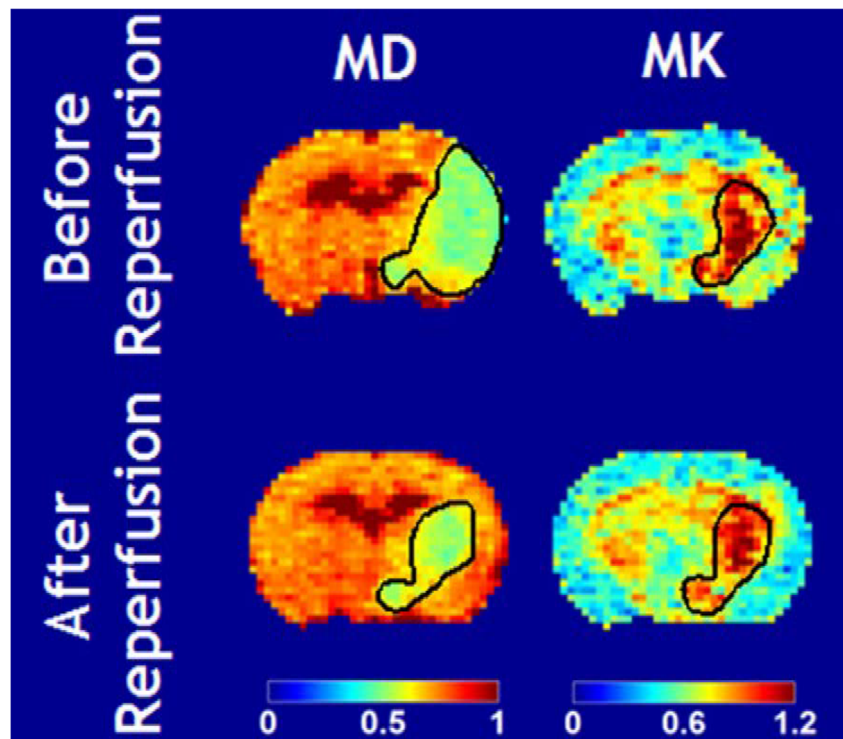
Building on the initial concept of perfusion/diffusion lesion mismatch, Kidwell et al. proposed a modified mismatch paradigm to refine the imaging definition of the ischemic penumbra [52]. The refined penumbra has its outer boundary smaller than the perfusion lesion, so the hypoperfused benign oligemia is excluded from the penumbra. Also, the modified penumbra’s inner boundary extends into the diffusion lesion to include a portion of diffusion lesion that is potentially salvageable [70]. Although the modified mismatch paradigm based on clinical observation is highly plausible, there has been a lack of stroke imaging techniques to reliably characterize the heterogeneous ischemic tissue to refine the penumbra definition. The development of advanced stroke imaging techniques could improve the identification of salvageable tissues, leading to the development of new clinical protocols and monitoring therapeutic strategies.

Emerging Stroke Imaging Methods—Diffusion Kurtosis Imaging

The ADC calculation assumes a monoexponential decay of MRI signal versus diffusion b value [71–73]. However, diffusion in biological tissue does not precisely follow a Gaussian free diffusion profile due to displacement restriction and barriers [74]. Kurtosis is an index that describes the degree of non-Gaussian diffusion that has been overlooked in routine diffusion MRI. Diffusion kurtosis imaging (DKI) quantifies not only the diffusion rate (i.e., diffusivity) but also the degree of deviation from the Gaussian diffusion profile (i.e., kurtosis) [75–78]. In a study of acute/subacute ischemic stroke patients, Hui concluded that ischemia preferentially alters the intra-axonal environment and proposed focal enlargement of axons known as axonal swelling or beading as a potential mechanism for kurtosis change following stroke [79].

It has been shown that in a transient middle cerebral artery occlusion (MCAO) rat model, the DWI lesion without kurtosis abnormality renormalizes after early reperfusion. In contrast, the kurtosis lesion within the DWI lesion shows a poor response to reperfusion [80]. Briefly, Fig. 2 shows mean diffusivity (MD) and kurtosis (MK) images before and after reperfusion in rats, documenting partial diffusion lesion renormalization. The MD lesion was considerably larger than

Fig. 2 DKI predicts diffusion renormalization after early (90-min MCAO) reperfusion (Cheung et al. Stroke 2012:2252–4)



the MK lesion during MCAO. After reperfusion (90-min MCAO), the MD lesion partially reversed to about the same size as the acute MK lesion during MCAO. In contrast, the MK lesion had little change before and after reperfusion. This observation suggests that the routine DWI lesion is heterogeneous, and DKI may distinguish the irreversibly damaged infarction core from the portion of potentially reversible DWI lesions. Such experimental stroke finding is consistent with the clinical observation that early recanalization in acute stroke patients often results in partial DWI reversibility that is correlated with functional outcomes [64, 81]. Although the routine DKI protocol requires a minimum of 31 scans, a fast DKI protocol has been developed that requires 13 scans, reducing the scan time by over 50% [82–84]. The diffusion/kurtosis mismatch region has shown a trend of higher perfusion than the infarction core [85]. Because it has been reported that thresholding ADC does not predict DWI reversibility [86], DKI and DWI likely capture different aspects of ischemic tissue injury, complementing each other. The use of DKI to define infarction core potentially avoids the overestimation of irreversibly damaged infarction tissue and allows for an accurate depiction of ischemic penumbra for EVT in an extended recanalization window.

Emerging Stroke Imaging Methods—Tissue pH

Acidosis is associated with oxygen–glucose deprivation and is a surrogate marker for energetic disruption in ischemic tissue [87, 88]. Cytosolic pH drop causes intracellular Na^+

accumulation, which subsequently increases Ca^{2+} by the $\text{Na}^+/\text{Ca}^{2+}$ exchanger [89, 90]. Calcium overload contributes to cell death. Under normal physiological conditions, tissue pH is relatively uniform and stable; however, abnormal glucose and oxygen metabolism changes the tissue pH during acute ischemic stroke. Indeed, pH is one of the last indices to change before ischemic tissue progresses towards infarction [28, 91]. A set of optical imaging studies have shown that acidic foci may recruit the ischemic penumbra into infarction [92]. Regi et al. showed that regional cerebral and cortical blood flows are not different between the permanent stroke (60 min) group and another transient ischemia group of four repeated ischemic episodes, 15 min each separated by 5-min reperfusion. At the same time, pH was significantly different [93]. This observation suggests that pH had greater power to define different severity of ischemic tissue injury. However, pH imaging is either invasive [94–98] or of insufficient spatiotemporal resolution for the acute stroke setting [99–101].

Amide Proton Transfer pH-Sensitive MRI

Amide proton transfer (APT) imaging, a specific form of chemical exchange saturation transfer (CEST) MRI, has been developed for pH imaging by sensitizing to pH-dependent chemical exchanges between amide protons from endogenous mobile proteins/peptides and water protons [102–110]. The endogenous amide proton chemical exchange is dominantly base-catalyzed in the brain, and APT MRI can be used as a sensitive non-invasive pH measurement technique within the

physiologically relevant pH [111–113]. pH imaging may help define the ischemic penumbra where hypoperfused tissue with intact pH corresponds to benign oligemia. In contrast, the hypoperfused tissue with pH drop identifies metabolic penumbra that is at risk of infarction. The use of pH mapping enables refining the perfusion/diffusion lesion mismatch into acidosis-based penumbra (concurrent perfusion and pH drop) and benign oligemia (hypoperfused tissue with little pH change) [114, 115]. Such additional pH-sensitive metabolic imaging along with the diffusion and perfusion MRI may improve prediction of tissue outcome and ultimately help guide stroke treatment [116].

Substantial progress has been achieved in fast pH MRI to make it amenable in the acute stroke setting. It has been shown that an intermediate RF saturation power level maximizes the pH contrast between the ischemic lesion and the contralateral normal area [117]. The pH-dependent APT MRI effect correlates with lactate concentration, as expected [118]. However, the commonly used pH-weighted image is susceptible to concomitant relaxation and magnetization transfer (MT) that are not pH specific. Zhou et al. showed that T_1 -normalized CEST effects for the intact white and gray matters are about equal for pH-dependent APT contrast. Yet, MT contrast asymmetry and nuclear overhauser enhancement (NOE) effects are significantly different [119]. Manual lesion outlining has been chosen to overcome pH-weighted image heterogeneity not

specific to pH for segmenting ischemic lesions in pH-weighted images [114]. To correct the pH-independent background heterogeneity, Guo et al. postulated that MTR_{asym} (Fig. 3a) heterogeneity from the intact tissue could be described as a multilinear regression (Fig. 3b) of magnetization transfer ratio (MTR) and relaxation (i.e., $1/T_1$), and dubbed it magnetization transfer and relaxation-normalized APT (MRAPT) analysis [120]. The development of MRAPT analysis improves pH imaging specificity and enables absolute pH mapping [121]. Perfusion and diffusion images (Fig. 3d and f) reveal pronounced perfusion, pH, and diffusion lesion mismatch, which have been postulated to correspond to infarction (diffusion lesion—black, Fig. 3f), metabolic penumbra (pH/diffusion mismatch—green, Fig. 3f), and benign oligemia (perfusion/pH mismatch—red, Fig. 3f). It is worth noting that the diffusion lesion has a worse pH drop than the penumbra [122]. Also, kurtosis lesion suffers from worse pH drop than that of the diffusion/kurtosis lesion mismatch, corroborating the refined mismatch paradigm [123]. Also, the pH-specific MRI allows fast field inhomogeneity correction that minimizes the acquisition time, which makes it highly amenable to the acute stroke setting [124, 125].

Wang et al. demonstrated the potential use of pH lesion in refining acute ischemic tissue in acute stroke rat models [121]. Figure 4 overlays multiparametric MRI indices from the diffusion lesion (black triangle), pH/diffusion lesion mismatch

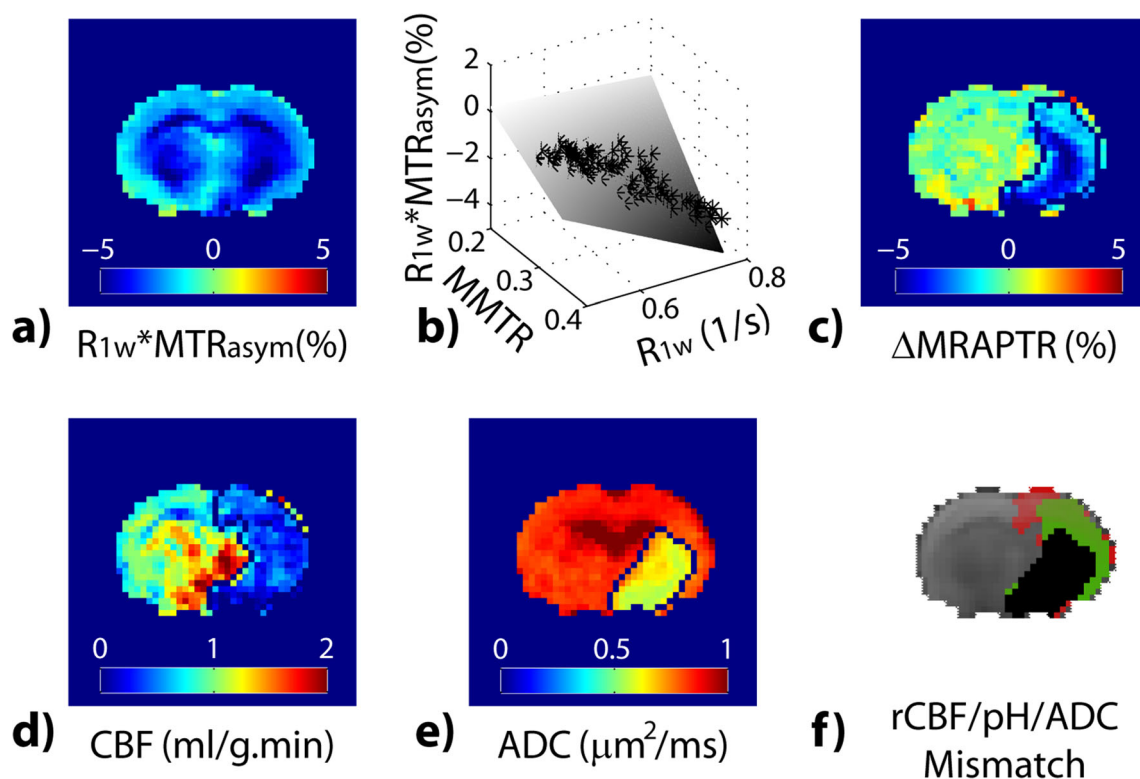
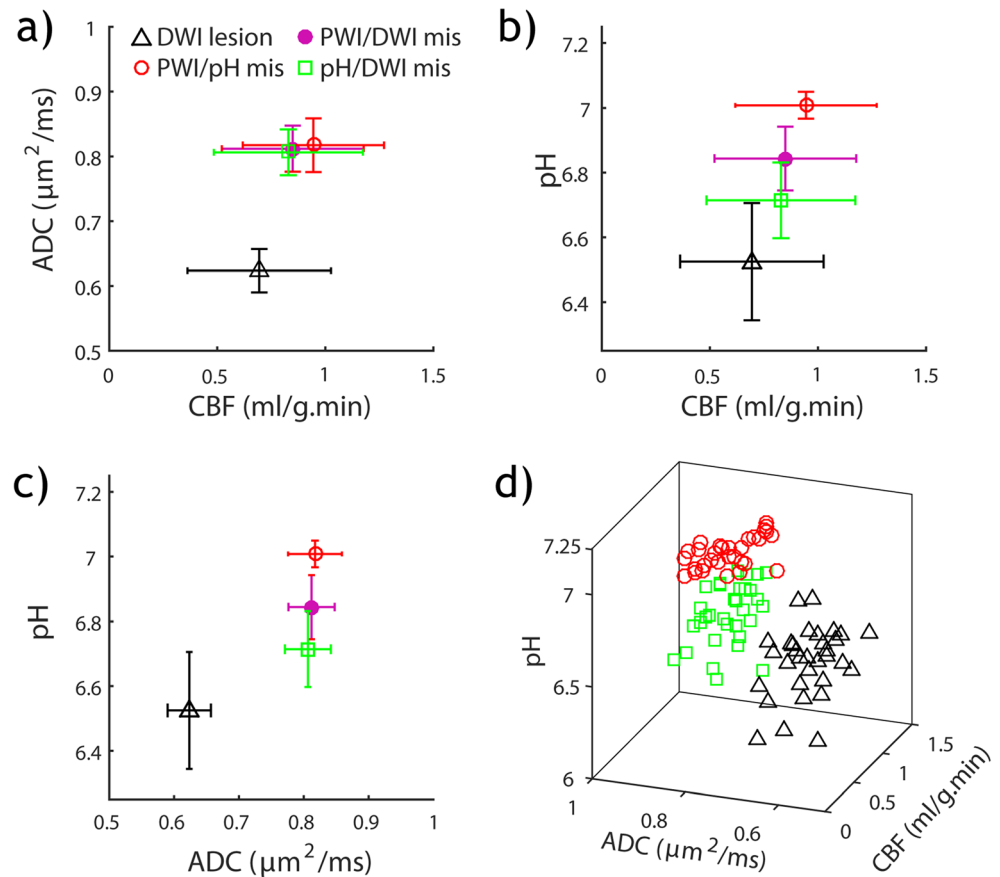


Fig. 3 Demonstration of pH-specific MRI in an acute stroke rat. **a** pH-weighted MTR_{asym} . **b** The multilinear regression between MTR_{asym} , R_{1w} , and MMTR from the intact tissue, per pixel, correction of which results in

c pH-specific $\Delta MRAPTR$ map. Rat perfusion (**d**) and diffusion (**e**) images reveal perfusion/pH/diffusion lesion mismatch (Guo et al., Neuroimage 2016:242–9)

Fig. 4 Comparison of perfusion, pH and diffusion indices from diffusion lesion, pH/diffusion lesion mismatch, perfusion/pH lesion mismatch, and perfusion/diffusion mismatch from all animals. **a** ADC vs. CBF. **b** pH vs. CBF. **c** pH vs. ADC. **d** Three-dimensional stratification of CBF, ADC, and pH indices from diffusion lesion, pH/diffusion lesion mismatch, and perfusion/pH lesion mismatch. CBF, cerebral blood flow; ADC, apparent diffusion coefficient



(green square), perfusion/pH lesion mismatch (red circle), and perfusion/diffusion lesion mismatch (solid pink circle). Figure 4a shows that although diffusion lesion has significantly reduced ADC from all three mismatch regions (i.e., pH/diffusion, perfusion/pH, and perfusion/diffusion mismatches), the mismatch regions have substantially overlapped perfusion and diffusion values. Although all ischemic areas have significantly reduced cerebral blood flow (CBF) from the contralateral brain, only PWI/pH mismatch has a significantly higher perfusion level than the diffusion lesion (Fig. 4b). Figure 4c shows that while ADC cannot differentiate perfusion/diffusion, perfusion/pH, and pH/diffusion mismatches, their pH was significantly different, being 6.84 ± 0.10 , 7.01 ± 0.04 , and 6.71 ± 0.12 , respectively. This data suggests the potential use of pH to sensitize the heterogeneous metabolic disruption within the routine PWI/DWI lesion mismatch. Indeed, Fig. 4d shows that regions of diffusion lesion, pH/DWI lesion mismatch, and PWI/pH lesion mismatch can be clustered using multi-dimensional perfusion, pH, and diffusion indices, augmenting routine perfusion and diffusion-based stroke imaging.

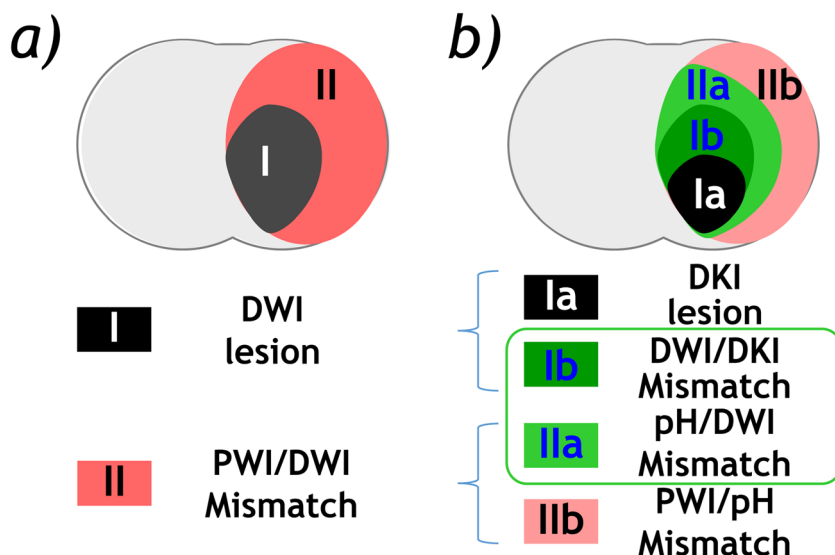
It is worth noting that there could be non-negligible T_1 changes following the acute stroke [126–128], while the mean MT ratio (MMTR) from ± 3.5 ppm shows little change [121]. After accounting for the difference in relaxation time, a recent study showed that the pH-sensitive APT signal dominates the

NOE effect, supporting the continued use of MTR_{asym} and amalgamations of it (e.g., MRAPT analysis) for pH imaging in the acute stroke setting [129].

New Imaging-Based Ischemic Tissue Classification

The recent development of DKI and pH MRI provides a tangible means to refine the mismatch paradigm (Fig. 5). Figure 5a shows the routine PWI/DWI mismatch paradigm, in which the DWI lesion defines the infarction core (black), and the PWI/DWI lesion mismatch identifies the salvageable penumbra tissue (red). With the development of DKI and pH imaging, we postulate that the heterogeneous ischemic lesion can be refined (Fig. 5b). Specifically, the PWI/DWI mismatch includes benign oligemia (hypoperfusion tissue without pH change, region IIb in red) and metabolic penumbra (hypoperfused acidic tissue, region IIa in light green). In addition, the DWI lesion contains an irreversible infarction core (DKI lesion, region Ia in black) and a portion of DWI lesion that is still salvageable despite its worse pH drop than region IIa (DWI/DKI lesion mismatch, region Ib in dark green). Altogether, the penumbra is defined by pH/DKI lesion mismatch (regions Ib (dark green) + region IIa (light green)). Although additional work is needed to fully establish that pH/DKI mismatch is the penumbra, accumulating data

Fig. 5 Illustration of the refined mismatch paradigm. **a** The routine PWI/DWI mismatch paradigm. **b** Modified penumbra defined by pH/DKI mismatch



suggest that advanced stroke imaging has the potential to augment the routine perfusion/diffusion mismatch paradigm. A fast and refined tissue characterization may provide the urgently needed imaging evidence to individualize and transform the state-of-the-art stroke patient care.

Clinical Translation of DKI and pH Imaging

Although it may seem challenging to incorporate advanced MRI to the acute stroke clinical settings, there have been

increasing reports of DKI and pH stroke imaging, particularly in large stroke centers where the infrastructure and workflow enable exploration of novel stroke imaging and treatment. Specifically, pH-sensitive APT MRI has been translated to study acute stroke patients with preliminary yet promising results, especially for those with relatively delayed presentation of 24–48 h [130–133]. For example, Heo et al. demonstrated pH-sensitive imaging in acute stroke patients at 3 T, with a scan time of 3 min 14 s [133]. Because the simplistic MTR_{asym} index includes contributions from APT, NOE, and

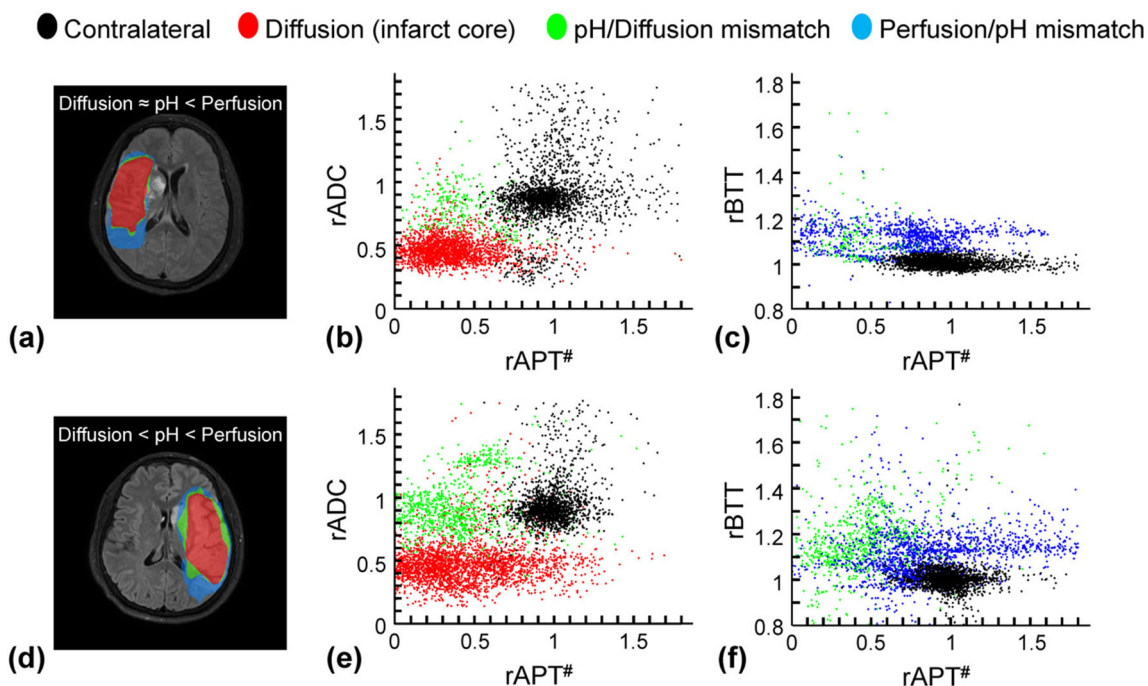


Fig. 6 Comparisons of diffusion/pH/perfusion deficits, pH/diffusion, and perfusion/pH scatterplots in two acute stroke patients at 1 day from symptom onset. **a–c** A patient with pH/perfusion mismatch, but minor diffusion/pH mismatch. **d–f** A patient with pH/perfusion mismatch, as

well as diffusion/pH mismatch. The distributions of the diffusion deficit area (red), pH–diffusion mismatch (green), and perfusion–pH mismatch (blue) were markedly different from those of the contralateral normal tissue (black)

possibly relaxation changes, the APT effect was quantified using an extrapolated semisolid MT reference signal technique (rAPT#). The pH/diffusion and perfusion/pH scatter plots from two representative stroke patients are shown in Fig. 6. The first patient had a perfusion/pH lesion mismatch with minor pH/diffusion mismatch (Fig. 6a). The scatter plot showed two clusters; the diffusion lesion showed significantly relative ADC (rADC) drop (Fig. 6b), while the perfusion/pH lesion mismatch showed intact rADC and delayed relative bolus transit time (rBTT), as expected (Fig. 6c). In the second stroke patient, there were both noticeable pH/diffusion and perfusion/pH lesion mismatches (Fig. 6d). The rADC and rAPT# scatter plots show that the pH/diffusion lesion mismatch is of higher rADC than the diffusion lesion (Fig. 6d). Although pH/diffusion lesion mismatch has lower rAPT# than the contralateral normal tissue, the pH/diffusion lesion mismatch and diffusion lesion had reasonably overlapped pH-weighted MRI contrast. Also, pH/diffusion and perfusion/pH lesion mismatches displayed delayed bolus transit time (Fig. 6f).

For the clinical translation of DKI, Yin et al. implemented a multi-band fast DKI protocol at 3 T, with a scan time of 2 min 10 s. They reported that for ischemic lesions over 1 cm in diameter, kurtosis lesions are of stronger correlation with the follow-up T2 MRI than those of diffusion MRI [134]. Also, Zhu et al. studied 156 stroke patients and analyzed 199 lesions in regions of periventricular white matter, corpus callosum, cerebellum, basal ganglia and thalamus, brainstem, and gray–white matter junctions. They concluded that DKI could reveal the differences in microstructure changes among various locations affected by acute ischemic stroke and performed better than diffusivity [135]. Guo et al. compared MK, axial kurtosis, and radial kurtosis in acute stroke patients. They concluded that axial kurtosis is better suited for diagnosing acute ischemic lesions in highly anisotropic brain regions, such as the corpus callosum and corona radiata. In contrast, MK may be appropriate for the lesions in low anisotropic or isotropic brain regions, such as the thalamus, subcortical white matter, and cerebral cortices [136].

Future Directions for Acute Stroke Imaging and Acute Stroke Research

Advanced imaging may help guide the development of new stroke therapeutics such as novel neuroprotection in combination with effective reperfusion like alkalinizing agents [137], Na⁺/H⁺ exchanger (NHE1) [138, 139], and acid-sensing ion channel (ASIC) blockers [140, 141]. In particular, the most recent Stroke Preclinical Assessment Network (SPAN) aims to test new compounds/interventions in animal models of cerebral ischemia following the stroke treatment academic industry roundtable recommendations [142–145]. Future work to reduce the scan time for DKI and pH imaging is needed to

enable a full panel of stroke MRI examinations without delaying the treatment. Advanced stroke imaging could also facilitate their translation and benefit new acute stroke trials, building on the successes of DAWN and DEFUSE-3.

Funding This study was supported in part by grants from NIH/NINDS 2R01NS083654 (to Sun) and Emory University Synergy Grant (to Hu and Sun).

Compliance with Ethical Standards

Conflict of Interest The authors declare that they have no conflict of interest.

Ethical Approval All applicable international, national, and institutional guidelines for the care and use of animals were followed. This article does not contain any studies with human participants performed by any of the authors.

References

1. Benjamin EJ, Muntner P, Alonso A, Bittencourt MS, Callaway CW, Carson AP, et al. Heart Disease and Stroke Statistics-2019 update: a report from the American Heart Association. *Circulation*. 2019;139(10):e56–e528.
2. Campbell BCV, de Silva DA, Macleod MR, Coutts SB, Schwamm LH, Davis SM, et al. Ischaemic stroke. *Nat Rev Dis Primers*. 2019;5(1):70.
3. Moussaddy A, Demchuk AM, Hill MD. Thrombolytic therapies for ischemic stroke: triumphs and future challenges. *Neuropharmacology*. 2018;134:272–9.
4. Heit JJ, Zaharchuk G, Wintermark M. Advanced neuroimaging of acute ischemic stroke: penumbra and collateral assessment. *Neuroimaging Clin N Am*. 2018;28(4):585–97.
5. Catanese L, Tarsia J, Fisher M. Acute ischemic stroke therapy overview. *Circ Res*. 2017;120(3):541–58.
6. Vilela P, Rowley HA. Brain ischemia: CT and MRI techniques in acute ischemic stroke. *Eur J Radiol*. 2017;96:162–72.
7. NINDS rt-PA Stroke Group. Tissue plasminogen activator for acute ischemic stroke. *N Engl J Med*. 1995;333:1581–7.
8. Vert C, Parra-Fariñas C, Rovira À. MR imaging in hyperacute ischemic stroke. *Eur J Radiol*. 2017;96:125–32.
9. Yang S-H, Lou M, Luo B, Jiang WJ, Liu R. Precision medicine for ischemic stroke, let us move beyond time is brain. *Transl Stroke Res*. 2018;9(2):93–5.
10. Wu L, Wu W, Tali ET, Yuh WT. Oligemia, penumbra, infarction: understanding hypoperfusion with neuroimaging. *Neuroimaging Clin N Am*. 2018;28(4):599–609.
11. Nogueira RG, Jadhav AP, Haussen DC, Bonafe A, Budzik RF, Bhuva P, et al. Thrombectomy 6 to 24 hours after stroke with a mismatch between deficit and infarct. *N Engl J Med*. 2017;378(1):11–21.
12. Albers GW, Marks MP, Kemp S, Christensen S, Tsai JP, Ortega-Gutierrez S, et al. Thrombectomy for stroke at 6 to 16 hours with selection by perfusion imaging. *N Engl J Med*. 2018;378(8):708–18.
13. Desai SM, Rocha M, Molyneaux BJ, Starr M, Kenmuir CL, Gross BA, et al. Thrombectomy 6–24 hours after stroke in trial ineligible patients. *J NeuroIntervent Surg*. 2018;10(11):1033–7.
14. Fisher M, Xiong Y. Evaluating patients for thrombectomy. *Brain Circ*. 2018;4(4):153–9.

15. Thomalla G, Simonsen CZ, Boutitie F, Andersen G, Berthezene Y, Cheng B, et al. MRI-guided thrombolysis for stroke with unknown time of onset. *N Engl J Med*. 2018;379(7):611–22.
16. Aoki J, Kimura K, Iguchi Y, Shibazaki K, Sakai K, Iwanaga T. FLAIR can estimate the onset time in acute ischemic stroke patients. *J Neurol Sci*. 2010;293(1–2):39–44.
17. Yoo AJ, Hakimelahi R, Rost NS, Schaefer PW, Hirsch JA, Gonzalez RG, et al. Diffusion weighted imaging reversibility in the brainstem following successful recanalization of acute basilar artery occlusion. *J Neurointerv Surg*. 2010;2(3):195–7.
18. Puig J, Shankar J, Liebeskind D, Terceño M, Nael K, Demchuk AM, et al. From “time is brain” to “imaging is brain”: a paradigm shift in the management of acute ischemic stroke. *J Neuroimaging*. 2020;30:562–71.
19. Leslie-Mazwi TM, Lev MH, Schaefer PW, Hirsch JA, González RG. MR imaging selection of acute stroke patients with emergent large vessel occlusions for thrombectomy. *Neuroimaging Clin N Am*. 2018;28(4):573–84.
20. Kidwell CS, Hsia AW. Imaging of the brain and cerebral vasculature in patients with suspected stroke: advantages and disadvantages of CT and MRI. *Curr Neurol Neurosci Rep*. 2006;6(1):9–16.
21. Leslie-Mazwi TM, Hirsch JA, Falcone GJ, Schaefer PW, Lev MH, Rabinov JD, et al. Endovascular stroke treatment outcomes after patient selection based on magnetic resonance imaging and clinical criteria. *JAMA Neurol*. 2016;73(1):43–9.
22. McTaggart RA, Yaghi S, Sacchetti DC, Haas RA, Hemendinger M, Arcuri D, et al. Mechanical embolectomy for acute ischemic stroke beyond six hours from symptom onset using MRI based perfusion imaging. *J Neurol Sci*. 2017;375:395–400.
23. Menjot de Champfleury N, et al. Efficacy of stent-retriever thrombectomy in magnetic resonance imaging versus computed tomographic perfusion-selected patients in SWIFT PRIME trial (solitaire FR with the intention for thrombectomy as primary endovascular treatment for acute ischemic stroke). *Stroke*. 2017;48(6):1560–6.
24. Almiri W, Meyer L, Politi M, Papanagioutou P. Diagnostic imaging of acute ischemic stroke. *Radiologe*. 2019;59(7):603–9.
25. Bateman M, Slater LA, Leslie-Mazwi T, Simonsen CZ, Stuckey S, Chandra RV. Diffusion and perfusion MR imaging in acute stroke: clinical utility and potential limitations for treatment selection. *Top Magn Reson Imaging*. 2017;26(2):77–82.
26. Dijkhuizen RM, van der Marel K, Otte WM, Hoff EI, van der Zijden JP, van der Toorn A, et al. Functional MRI and diffusion tensor imaging of brain reorganization after experimental stroke. *Transl Stroke Res*. 2012;3(1):36–43.
27. Nael K, et al. Six-minute magnetic resonance imaging protocol for evaluation of acute ischemic stroke. *Stroke*. 2014;45(7):1985–91.
28. Hossmann KA. Viability thresholds and the penumbra of focal ischemia. *Ann Neurol*. 1994;36(4):557–65.
29. Back T. Pathophysiology of the ischemic penumbra—revision of a concept. *Cell Mol Neurobiol*. 1998;18(6):621–38.
30. Markus HS. Cerebral perfusion and stroke. *J Neurol Neurosurg Psychiatry*. 2004;75(3):353–61.
31. Williams SR, Proctor E, Allen K, Gadian DG, Crockard HA. Quantitative estimation of lactate in the brain by ¹H NMR. *Magn Reson Med*. 1988;7(4):425–31.
32. Terrier F, et al. Lactate mapping in ischemic rat kidneys using ¹H spectroscopic imaging. *Investig Radiol*. 1992;27(4):282–6.
33. Dijkhuizen RM, de Graaf RA, Garwood M, Tulleken KAF, Nicolay K. Spatial assessment of the dynamics of lactate formation in focal ischemic rat brain. *J Cereb Blood Flow Metab*. 1999;19(4):376–9.
34. Hyder F, Rothman DL. Advances in imaging brain metabolism. *Annu Rev Biomed Eng*. 2017;19(1):485–515.
35. Obrenovitch TP, Garofalo O, Harris RJ, Bordi L, Ono M, Momma F, et al. Brain tissue concentrations of ATP, phosphocreatine, lactate, and tissue pH in relation to reduced cerebral blood flow following experimental acute middle cerebral artery occlusion. *J Cereb Blood Flow Metab*. 1988;8(6):866–74.
36. Paschen W, Djuricic B, Mies G, Schmidt-Kastner R, Linn F. Lactate and pH in the brain: association and dissociation in different pathophysiological states. *J Neurochem*. 1987;48(1):154–9.
37. Allen K, Busza AL, Crockard HA, Frackowiak RSJ, Gadian DG, Proctor E, et al. Acute cerebral ischaemia: concurrent changes in cerebral blood flow, energy metabolites, pH, and lactate measured with hydrogen clearance and ³¹P and ¹H nuclear magnetic resonance spectroscopy. III. Changes following ischaemia. *J Cereb Blood Flow Metab*. 1988;8(6):816–21.
38. Katsura K, Asplund B, Ekholm A, Siesjö BK. Extra- and intracellular pH in the brain during ischaemia, related to tissue lactate content in normo- and hypercapnic rats. *Eur J Neurosci*. 1992;4(2):166–76.
39. Göttler J, Kaczmarz S, Kallmayer M, Wustrow I, Eckstein HH, Zimmer C, et al. Flow-metabolism uncoupling in patients with asymptomatic unilateral carotid artery stenosis assessed by multi-modal magnetic resonance imaging. *J Cereb Blood Flow Metab*. 2018;39(11):2132–43.
40. Smith AG, Hill CR. Imaging assessment of acute ischaemic stroke: a review of radiological methods. *Br J Radiol*. 2018;91(1083):20170573.
41. An H, Ford AL, Vo K, Powers WJ, Lee JM, Lin W. Signal evolution and infarction risk for apparent diffusion coefficient lesions in acute ischemic stroke are both time- and perfusion-dependent. *Stroke*. 2011;42(5):1276–81.
42. Bonney PA, et al. The continued role and value of imaging for acute ischemic stroke. *Neurosurgery*. 2019;85(suppl_1):S23–30.
43. Olivot J-M, Mosimann PJ, Labreuche J, Inoue M, Meseguer E, Desilles JP, et al. Impact of diffusion-weighted imaging lesion volume on the success of endovascular reperfusion therapy. *Stroke*. 2013;44(8):2205–11.
44. Rordorf G, Koroshetz WJ, Copen WA, Cramer SC, Schaefer PW, Budzik RF, et al. Regional ischemia and ischemic injury in patients with acute middle cerebral artery stroke as defined by early diffusion-weighted and perfusion-weighted MRI. *Stroke*. 1998;29(5):939–43.
45. Schaefer PW, et al. Assessing tissue viability with MR diffusion and perfusion imaging. *AJNR Am J Neuroradiol*. 2003;24(3):436–43.
46. Wu O, Ostergaard L, Sorensen AG. Technical aspects of perfusion-weighted imaging. *Neuroimaging Clin N Am*. 2005;15(3):623–37 xi.
47. Alsop DC, Detre JA, Golay X, Günther M, Hendrikse J, Hernandez-Garcia L, et al. Recommended implementation of arterial spin-labeled perfusion MRI for clinical applications: a consensus of the ISMRM perfusion study group and the European consortium for ASL in dementia. *Magn Reson Med*. 2015;73(1):102–16.
48. Haller S, Zaharchuk G, Thomas DL, Lovblad KO, Barkhof F, Golay X. Arterial spin labeling perfusion of the brain: emerging clinical applications. *Radiology*. 2016;281(2):337–56.
49. Bokkers RP, Hernandez DA, Merino JG, Mirasol RV, van Osch M, Hendrikse J, et al. Whole-brain arterial spin labeling perfusion MRI in patients with acute stroke. *Stroke*. 2012;43(5):1290–4.
50. Wang DJJ, Alger JR, Qiao JX, Hao Q, Hou S, Fiaz R, et al. The value of arterial spin-labeled perfusion imaging in acute ischemic stroke: comparison with dynamic susceptibility contrast-enhanced MRI. *Stroke*. 2012;43(4):1018–24.
51. Wintermark M, et al. Comparative overview of brain perfusion imaging techniques. *Stroke*. 2005;36(9):e83–99.
52. Kidwell CS, Alger JR, Saver JL. Evolving paradigms in neuroimaging of the ischemic penumbra. *Stroke*. 2004;35(11 Suppl 1):2662–5.

53. Schlaug G, Benfield A, Baird AE, Siewert B, Lovblad KO, Parker RA, et al. The ischemic penumbra: operationally defined by diffusion and perfusion MRI. *Neurology*. 1999;53(7):1528–37.
54. Wu O, Koroshetz WJ, Østergaard L, Buonanno FS, Copen WA, Gonzalez RG, et al. Predicting tissue outcome in acute human cerebral ischemia using combined diffusion- and perfusion-weighted MR imaging. *Stroke*. 2001;32(4):933–42.
55. Bristow MS, Simon JE, Brown RA, Eliasziw M, Hill MD, Coutts SB, et al. MR perfusion and diffusion in acute ischemic stroke: human gray and white matter have different thresholds for infarction. *J Cereb Blood Flow Metab*. 2005;25(10):1280–7.
56. Arakawa S, Wright PM, Koga M, Phan TG, Reutens DC, Lim I, et al. Ischemic thresholds for gray and white matter: a diffusion and perfusion magnetic resonance study. *Stroke*. 2006;37(5):1211–6.
57. Shin W, Horowitz S, Ragin A, Chen Y, Walker M, Carroll TJ. Quantitative cerebral perfusion using dynamic susceptibility contrast MRI: evaluation of reproducibility and age- and gender-dependence with fully automatic image postprocessing algorithm. *Magn Reson Med*. 2007;58(6):1232–41.
58. Zaharchuk G. Arterial spin label imaging of acute ischemic stroke and transient ischemic attack. *Neuroimaging Clin N Am*. 2011;21(2):285–301 x.
59. Kidwell CS, Alger JR, Saver JL. Beyond mismatch: evolving paradigms in imaging the ischemic penumbra with multimodal magnetic resonance imaging. *Stroke*. 2003;34(11):2729–35.
60. Nicoli F, Lefur Y, Denis B, Ranjeva JP, Confort-Gouny S, Cozzone PJ. Metabolic counterpart of decreased apparent diffusion coefficient during hyperacute ischemic stroke: a brain proton magnetic resonance spectroscopic imaging study. *Stroke*. 2003;34(7):e82–7.
61. Geisler BS, Brandhoff F, Fiehler J, Saager C, Speck O, Röther J, et al. Blood-oxygen-level-dependent MRI allows metabolic description of tissue at risk in acute stroke patients. *Stroke*. 2006;37(7):1778–84.
62. An H, Liu Q, Chen Y, Lin W. Evaluation of MR-derived cerebral oxygen metabolic index in experimental hyperoxic hypercapnia, hypoxia, and ischemia. *Stroke*. 2009;40(6):2165–72.
63. Kidwell CS, Saver JL, Mattiello J, Starkman S, Vinuela F, Duckwiler G, et al. Thrombolytic reversal of acute human cerebral ischemic injury shown by diffusion/perfusion magnetic resonance imaging. *Ann Neurol*. 2000;47(4):462–9.
64. Labeyrie MA, Turc G, Hess A, Hervé P, Mas JL, Meder JF, et al. Diffusion lesion reversal after thrombolysis: a MR correlate of early neurological improvement. *Stroke*. 2012;43(11):2986–91.
65. Soize S, Tisserand M, Charron S, Turc G, Ben Hassen W, Labeyrie MA, et al. How sustained is 24-hour diffusion-weighted imaging lesion reversal? Serial magnetic resonance imaging in a patient cohort thrombolysed within 4.5 hours of stroke onset. *Stroke*. 2015;46(3):704–10.
66. Tisserand M, Turc G, Charron S, Legrand L, Edjlali M, Seners P, et al. Does diffusion lesion volume above 70 mL preclude favorable outcome despite post-thrombolysis recanalization? *Stroke*. 2016;47(4):1005–11.
67. Inoue M, Mlynash M, Christensen S, Wheeler HM, Straka M, Tipirneni A, et al. Early diffusion-weighted imaging reversal after endovascular reperfusion is typically transient in patients imaged 3 to 6 hours after onset. *Stroke*. 2014;45(4):1024–8.
68. Yoo J, Choi JW, Lee SJ, Hong JM, Hong JH, Kim CH, et al. Ischemic diffusion lesion reversal after endovascular treatment. *Stroke*. 2019;50(6):1504–9.
69. Hsia AW, Luby M, Cullison K, Burton S, Armonda R, Liu AH, et al. Rapid apparent diffusion coefficient evolution after early revascularization. *Stroke*. 2019;50(8):2086–92.
70. Kohno K, Hoehn-Berlage M, Mies G, Back T, Hossmann KA. Relationship between diffusion-weighted MR images, cerebral blood flow, and energy state in experimental brain infarction. *Magn Reson Imaging*. 1995;13(1):73–80.
71. Hossmann KA, Fischer M, Bockhorst K, Hoehn-Berlage M. NMR imaging of the apparent diffusion coefficient (ADC) for the evaluation of metabolic suppression and recovery after prolonged cerebral ischemia. *J Cereb Blood Flow Metab*. 1994;14(5):723–31.
72. Norris D, Niendorf T, Leibfritz D. Health and infarcted brain tissues studied at short diffusion times: the origins of apparent restriction and the reduction in apparent diffusion coefficient. *NMR Biomed*. 1994;7(7):304–10.
73. Desmond PM, Lovell AC, Rawlinson AA, Parsons MW, Barber PA, Yang Q, et al. The value of apparent diffusion coefficient maps in early cerebral ischemia. *AJNR Am J Neuroradiol*. 2001;22(7):1260–7.
74. Jensen JH, Helpert JA. MRI quantification of non-Gaussian water diffusion by kurtosis analysis. *NMR Biomed*. 2010;23(7):698–710.
75. Weber RA, Hui ES, Jensen JH, Nie X, Falangola MF, Helpert JA, et al. Diffusional kurtosis and diffusion tensor imaging reveal different time-sensitive stroke-induced microstructural changes. *Stroke*. 2015;46(2):545–50.
76. Li C, Lan C, Zhang X, Yin L, Hao X, Tian J, et al. Evaluation of diffusional kurtosis imaging in sub-acute ischemic stroke: comparison with rehabilitation treatment effect. *Cell Transplant*. 2019;28(8):1053–61.
77. Zhang S, Zhu W, Zhang Y, Yao Y, Shi J, Wang CY, et al. Diffusional kurtosis imaging in evaluating the secondary change of corticospinal tract after unilateral cerebral infarction. *Am J Transl Res*. 2017;9(3):1426–34.
78. Hansen B, Jespersen SN. Recent developments in fast kurtosis imaging. *Front Phys*. 2017;5(40). <https://doi.org/10.3389/fphys.2017.00040>.
79. Hui ES, Fieremans E, Jensen JH, Tabesh A, Feng W, Bonilha L, et al. Stroke assessment with diffusional kurtosis imaging. *Stroke*. 2012;43(11):2968–73.
80. Cheung JS, Wang E, Lo EH, Sun PZ. Stratification of heterogeneous diffusion MRI ischemic lesion with kurtosis imaging: evaluation of mean diffusion and kurtosis MRI mismatch in an animal model of transient focal ischemia. *Stroke*. 2012;43(8):2252–4.
81. Fiehler J, Knudsen K, Kucinski T, Kidwell CS, Alger JR, Thomalla G, et al. Predictors of apparent diffusion coefficient normalization in stroke patients. *Stroke*. 2004;35(2):514–9.
82. Hansen B, Lund TE, Sangill R, Jespersen SN. Experimentally and computationally fast method for estimation of a mean kurtosis. *Magn Reson Med*. 2013;69(6):1754–60.
83. Wu Y, Kim J, Chan ST, Zhou IY, Guo Y, Igarashi T, et al. Comparison of image sensitivity between conventional tensor-based and fast diffusion kurtosis imaging protocols in a rodent model of acute ischemic stroke. *NMR Biomed*. 2016;29(5):625–30.
84. Zhou IY, Guo Y, Igarashi T, Wang Y, Mandeville E, Chan ST, et al. Fast diffusion kurtosis imaging (DKI) with Inherent COrrelation-based Normalization (ICON) enhances automatic segmentation of heterogeneous diffusion MRI lesion in acute stroke. *NMR Biomed*. 2016;29(12):1670–7.
85. Wang E, Wu Y, Cheung JS, Zhou IY, Igarashi T, Zhang XA, et al. pH imaging reveals worsened tissue acidification in diffusion kurtosis lesion than the kurtosis/diffusion lesion mismatch in an animal model of acute stroke. *J Cereb Blood Flow Metab*. 2017;37(10):3325–33.
86. Loh PS, Butcher KS, Parsons MW, MacGregor L, Desmond PM, Tress BM, et al. Apparent diffusion coefficient thresholds do not predict the response to acute stroke thrombolysis. *Stroke*. 2005;36(12):2626–31.

87. Astrup J, Siesjo BK, Symon L. Thresholds in cerebral ischemia—the ischemic penumbra. *Stroke*. 1981;12(6):723–5.
88. Sako K, Kobatake K, Yamamoto YL, Diksic M. Correlation of local cerebral blood flow, glucose utilization, and tissue pH following a middle cerebral artery occlusion in the rat. *Stroke*. 1985;16(5):828–34.
89. Siesjo BK. Pathophysiology and treatment of focal cerebral ischemia. Part II: Mechanisms of damage and treatment. *J Neurosurg*. 1992;77(3):337–54.
90. Jeffs GJ, Meloni BP, Bakker AJ, Knuckey NW. The role of the Na(+)/Ca(2+) exchanger (NCX) in neurons following ischaemia. *J Clin Neurosci*. 2007;14(6):507–14.
91. Uriá-Avellanal C, Robertson NJ. Na⁺/H⁺ exchangers and intracellular pH in perinatal brain injury. *Transl Stroke Res*. 2014;5(1):79–98.
92. Tomlinson FH, Anderson RE, Meyer FB. Brain pHi, cerebral blood flow, and NADH fluorescence during severe incomplete global ischemia in rabbits. *Stroke*. 1993;24(3):435–43.
93. Regli L, Anderson RE, Meyer FB. Effects of intermittent reperfusion on brain pHi, rCBF, and NADH during rabbit focal cerebral ischemia. *Stroke*. 1995;26(8):1444–51 discussion 1451–2.
94. Mutch WA, Hansen AJ. Extracellular pH changes during spreading depression and cerebral ischemia: mechanisms of brain pH regulation. *J Cereb Blood Flow Metab*. 1984;4(1):17–27.
95. Csiba L, Paschen W, Hossmann KA. A topographic quantitative method for measuring brain tissue pH under physiological and pathophysiological conditions. *Brain Res*. 1983;289(1–2):334–7.
96. LaManna JC. Intracellular pH determination by absorption spectrophotometry of neutral red. *Metab Brain Dis*. 1987;2(3):167–82.
97. Peek KE, Lockwood AH, Izumiya M, Yap EWH, Labove J. Glucose metabolism and acidosis in the metabolic penumbra of rat brain. *Metab Brain Dis*. 1989;4(4):261–72.
98. Khan T, Soller B, Naghavi M, Casscells W. Tissue pH determination for the detection of metabolically active, inflamed vulnerable plaques using near-infrared spectroscopy: an in-vitro feasibility study. *Cardiology*. 2005;103(1):10–6.
99. Adam WR, Koretsky AP, Weiner MW. ³¹P-NMR in vivo measurement of renal intracellular pH: effects of acidosis and K⁺ depletion in rats. *Am J Phys*. 1986;251(5 Pt 2):F904–10.
100. Hohn-Berlage M, et al. Imaging of brain tissue pH and metabolites. A new approach for the validation of volume-selective NMR spectroscopy. *NMR Biomed*. 1989;2(5–6):240–5.
101. Edden RA, et al. Optimized detection of lactate at high fields using inner volume saturation. *Magn Reson Med*. 2006;56(4):912–7.
102. Ward KM, Aletras AH, Balaban RS. A new class of contrast agents for MRI based on proton chemical exchange dependent saturation transfer (CEST). *J Magn Reson*. 2000;143(1):79–87.
103. Zhou J, Payen JF, Wilson DA, Traystman RJ, van Zijl PCM. Using the amide proton signals of intracellular proteins and peptides to detect pH effects in MRI. *Nat Med*. 2003;9(8):1085–90.
104. Sun PZ, Sorensen AG. Imaging pH using the chemical exchange saturation transfer (CEST) MRI: correction of concomitant RF irradiation effects to quantify CEST MRI for chemical exchange rate and pH. *Magn Reson Med*. 2008;60(2):390–7.
105. Sun PZ, Benner T, Copen WA, Sorensen AG. Early experience of translating pH-weighted MRI to image human subjects at 3 Tesla. *Stroke*. 2010;41(10 Suppl):S147–51.
106. Zong X, Wang P, Kim SG, Jin T. Sensitivity and source of amine-proton exchange and amide-proton transfer magnetic resonance imaging in cerebral ischemia. *Magn Reson Med*. 2014;71(1):118–32.
107. Li H, Zu Z, Zaiss M, Khan IS, Singer RJ, Gochberg DF, et al. Imaging of amide proton transfer and nuclear overhauser enhancement in ischemic stroke with corrections for competing effects. *NMR Biomed*. 2015;28(2):200–9.
108. Sun PZ, Xiao G, Zhou IY, Guo Y, Wu R. A method for accurate pH mapping with chemical exchange saturation transfer (CEST) MRI. *Contrast Media Mol Imaging*. 2016;11(3):195–202.
109. Jin T, Wang P, Hitchens TK, Kim SG. Enhancing sensitivity of pH-weighted MRI with combination of amide and guanidyl CEST. *Neuroimage*. 2017;157:341–50.
110. Wu Y, Zhou IY, Lu D, Manderville E, Lo EH, Zheng H, et al. pH-sensitive amide proton transfer effect dominates the magnetization transfer asymmetry contrast during acute ischemia-quantification of multipool contribution to in vivo CEST MRI. *Magn Reson Med*. 2018;79(3):1602–8.
111. Jokivarsi KT, Gröhn HI, Gröhn OH, Kauppinen RA. Proton transfer ratio, lactate, and intracellular pH in acute cerebral ischemia. *Magn Reson Med*. 2007;57(4):647–53.
112. Sun PZ, Wang E, Cheung JS. Imaging acute ischemic tissue acidosis with pH-sensitive endogenous amide proton transfer (APT) MRI-correction of tissue relaxation and concomitant RF irradiation effects toward mapping quantitative cerebral tissue pH. *Neuroimage*. 2012;60(1):1–6.
113. Jin T, Wang P, Zong X, Kim SG. MR imaging of the amide-proton transfer effect and the pH-insensitive nuclear overhauser effect at 9.4 T. *Magn Reson Med*. 2013;69(3):760–70.
114. Sun PZ, Zhou J, Sun W, Huang J, van Zijl PCM. Detection of the ischemic penumbra using pH-weighted MRI. *J Cereb Blood Flow Metab*. 2007;27(6):1129–36.
115. Zhou J, van Zijl PC. Defining an acidosis-based ischemic penumbra from pH-weighted MRI. *Transl Stroke Res*. 2011;3(1):76–83.
116. Dani KA, Warach S. Metabolic imaging of ischemic stroke: the present and future. *AJNR Am J Neuroradiol*. 2014;35(6 Suppl):S37–43.
117. Sun PZ, Zhou J, Huang J, van Zijl P. Simplified quantitative description of amide proton transfer (APT) imaging during acute ischemia. *Magn Reson Med*. 2007;57(2):405–10.
118. Sun PZ, Cheung JS, Wang E, Lo EH. Association between pH-weighted endogenous amide proton chemical exchange saturation transfer MRI and tissue lactic acidosis during acute ischemic stroke. *J Cereb Blood Flow Metab*. 2011;31(8):1743–50.
119. Zhou IY, Lu D, Ji Y, Wu L, Wang E, Cheung JS, et al. Determination of multipool contributions to endogenous amide proton transfer effects in global ischemia with high spectral resolution in vivo chemical exchange saturation transfer MRI. *Magn Reson Med*. 2019;81(1):645–52.
120. Guo Y, Zhou IY, Chan ST, Wang Y, Manderville ET, Igarashi T, et al. pH-sensitive MRI demarcates graded tissue acidification during acute stroke-pH specificity enhancement with magnetization transfer and relaxation-normalized amide proton transfer (APT) MRI. *Neuroimage*. 2016;141:242–9.
121. Wang E, Wu Y, Cheung JS, Igarashi T, Wu L, Zhang X, et al. Mapping tissue pH in an experimental model of acute stroke-determination of graded regional tissue pH changes with non-invasive quantitative amide proton transfer MRI. *NeuroImage*. 2019;191:610–7.
122. Back T, Hoehn-Berlage M, Kohno K, Hossmann KA. Diffusion nuclear magnetic resonance imaging in experimental stroke. Correlation with cerebral metabolites. *Stroke*. 1994;25(2):494–500.
123. Lu D, Jiang Y, Ji Y, Zhou IY, Manderville E, Lo EH, et al. Evaluation of diffusion kurtosis imaging of stroke lesion with hemodynamic and metabolic MRI in a rodent model of acute stroke. *AJR Am J Roentgenol*. 2018;210(4):720–7.
124. Sun PZ. Fast correction of B0 field inhomogeneity for pH-specific magnetization transfer and relaxation normalized amide proton transfer imaging of acute ischemic stroke without Z-spectrum. *Magn Reson Med*. 2020;83(5):1688–97.
125. Sun PZ. Demonstration of magnetization transfer and relaxation normalized pH-specific pulse-amide proton transfer imaging in an

- animal model of acute stroke. *Magn Reson Med.* 2020;84(3):1526–33.
126. Ewing JR, Jiang Q, Boska M, Zhang ZG, Brown SL, Li GH, et al. T_1 and magnetization transfer at 7 Tesla in acute ischemic infarct in the rat. *Magn Reson Med.* 1999;41(4):696–705.
 127. Zhang XY, Wang F, Afzal A, Xu J, Gore JC, Gochberg DF, et al. A new NOE-mediated MT signal at around -1.6ppm for detecting ischemic stroke in rat brain. *Magn Reson Imaging.* 2016;34(8):1100–6.
 128. McGarry BL, et al. Magnetic resonance imaging protocol for stroke onset time estimation in permanent cerebral ischemia. *J Vis Exp.* 2017;2017(127):56103. <https://doi.org/10.3791/55277>.
 129. Wu L, Jiang L, Sun PZ. Investigating the origin of pH-sensitive magnetization transfer ratio asymmetry MRI contrast during the acute stroke: correction of $T(1)$ change reveals the dominant amide proton transfer MRI signal. *Magn Reson Med.* 2020;84(5):2702–12.
 130. Tee YK, Harston GWJ, Blockley N, Okell TW, Levman J, Sheerin F, et al. Comparing different analysis methods for quantifying the MRI amide proton transfer (APT) effect in hyperacute stroke patients. *NMR Biomed.* 2014;27(9):1019–29.
 131. Harston GW, et al. Identifying the ischaemic penumbra using pH-weighted magnetic resonance imaging. *Brain.* 2015;138(Pt 1):36–42.
 132. Msayib Y, Harston GWJ, Tee YK, Sheerin F, Blockley NP, Okell TW, et al. Quantitative CEST imaging of amide proton transfer in acute ischaemic stroke. *Neuroimage Clin.* 2019;23:101833.
 133. Heo HY, Zhang Y, Burton TM, Jiang S, Zhao Y, van Zijl PCM, et al. Improving the detection sensitivity of pH-weighted amide proton transfer MRI in acute stroke patients using extrapolated semisolid magnetization transfer reference signals. *Magn Reson Med.* 2017;78(3):871–80.
 134. Yin J, Sun H, Wang Z, Ni H, Shen W, Sun PZ. Diffusion kurtosis imaging of acute infarction: comparison with routine diffusion and follow-up MR imaging. *Radiology.* 2018;287(2):651–7.
 135. Zhu L-H, Zhang ZP, Wang FN, Cheng QH, Guo G. Diffusion kurtosis imaging of microstructural changes in brain tissue affected by acute ischemic stroke in different locations. *Neural Regen Res.* 2019;14(2):272–9.
 136. Guo YL, Li SJ, Zhang ZP, Shen ZW, Zhang GS, Yan G, et al. Parameters of diffusional kurtosis imaging for the diagnosis of acute cerebral infarction in different brain regions. *Exp Ther Med.* 2016;12(2):933–8.
 137. Anderson RE, Meyer FB. Protection of focal cerebral ischemia by alkalinization of systemic pH. *Neurosurgery.* 2002;51(5):1256–65 discussion 1265–6.
 138. Chang HB, Gao X, Nepomuceno R, Hu S, Sun D. $Na(+)/H(+)$ exchanger in the regulation of platelet activation and paradoxical effects of cariporide. *Exp Neurol.* 2015;272:11–6.
 139. Song S, Wang S, Pigott VM, Jiang T, Foley LM, Mishra A, et al. Selective role of $Na(+)/H(+)$ exchanger in Cx3cr1(+) microglial activation, white matter demyelination, and post-stroke function recovery. *Glia.* 2018;66(11):2279–98.
 140. Xiong ZG, Zhu XM, Chu XP, Minami M, Hey J, Wei WL, et al. Neuroprotection in ischemia: blocking calcium-permeable acid-sensing ion channels. *Cell.* 2004;118(6):687–98.
 141. Pignataro G, Simon RP, Xiong ZG. Prolonged activation of ASIC1a and the time window for neuroprotection in cerebral ischaemia. *Brain.* 2007;130(Pt 1):151–8.
 142. McCabe C, Arroja MM, Reid E, Macrae IM. Animal models of ischaemic stroke and characterisation of the ischaemic penumbra. *Neuropharmacology.* 2018;134:169–77.
 143. Dhanesha N, Vázquez-Rosa E, Cintrón-Pérez CJ, Thedens D, Kort AJ, Chuong V, et al. Treatment with uric acid reduces infarct and improves neurologic function in female mice after transient cerebral ischemia. *J Stroke Cerebrovasc Dis.* 2018;27(5):1412–6.
 144. Shin HK, Huang PL, Ayata C. Rho-kinase inhibition improves ischemic perfusion deficit in hyperlipidemic mice. *J Cereb Blood Flow Metab.* 2014;34(2):284–7.
 145. Savitz SI, Baron JC, Fisher M, for the STAIR X Consortium, Albers GW, Arbe-Barnes S, et al. Stroke treatment academic industry roundtable X. *Stroke.* 2019;50(4):1026–31.

Publisher's Note Springer Nature remains neutral with regard to jurisdictional claims in published maps and institutional affiliations.